Acta Cryst E CRYSTALLOGRAPHIC COMMUNICATIONS

ISSN 2056-9890

Crystal structure, Hirshfeld surface analysis, interaction energy and DFT studies of (2*Z*)-2-(2,4-dichlorobenzylidene)-4-nonyl-3,4-dihydro-2*H*-1,4-benzothiazin-3-one

Brahim Hni,[a]* Nada Kheira Sebbar,[b,a] Tuncer Hökelek,[c] Achour Redouane,[a] Joel T. Mague,[d] Noureddine Hamou Ahabchane[a] and El Mokhtar Essassi[a]

[a]Laboratoire de Chimie Organique Hétérocyclique URAC 21, Pôle de Compétence Pharmacochimie, Av. Ibn Battouta, BP 1014, Faculté des Sciences, Université Mohammed V, Rabat, Morocco, [b]Laboratoire de Chimie Appliquée et Environnement, Equipe de Chimie Bioorganique Appliquée, Faculté des Sciences, Université Ibn Zohr, Agadir, Morocco, [c]Department of Physics, Hacettepe University, 06800 Beytepe, Ankara, Turkey, and [d]Department of Chemistry, Tulane University, New Orleans, LA 70118, USA. *Correspondence e-mail: brahimhni2018@gmail.com

Received 9 January 2020
Accepted 25 January 2020

Edited by A. J. Lough, University of Toronto, Canada

Keywords: crystal structure; 1,4-benzothiazin-3-one; dihydrothiazine; hydrogen bond; π-stacking; Hirshfeld surface.

CCDC reference: 1980073

Supporting information: this article has supporting information at journals.iucr.org/e

The title compound, $C_{24}H_{27}Cl_2NOS$, contains 1,4-benzothiazine and 2,4-dichlorophenylmethylidene units in which the dihydrothiazine ring adopts a screw-boat conformation. In the crystal, intermolecular $C-H_{Bnz}\cdots O_{Thz}$ (Bnz = benzene and Thz = thiazine) hydrogen bonds form chains of molecules extending along the *a*-axis direction, which are connected to their inversion-related counterparts by $C-H_{Bnz}\cdots Cl_{Dchlphy}$ (Dchlphy = 2,4-dichlorophenyl) hydrogen bonds and $C-H_{Dchlphy}\cdots\pi$ (ring) interactions. These double chains are further linked by $C-H_{Dchlphy}\cdots O_{Thz}$ hydrogen bonds, forming stepped layers approximately parallel to (012). The Hirshfeld surface analysis of the crystal structure indicates that the most important contributions for the crystal packing are from H···H (44.7%), C···H/H···C (23.7%), Cl···H/H···Cl (18.9%), O···H/H···O (5.0%) and S···H/H···S (4.8%) interactions. Hydrogen-bonding and van der Waals interactions are the dominant interactions in the crystal packing. Computational chemistry indicates that in the crystal, $C-H_{Dchlphy}\cdots O_{Thz}$, $C-H_{Bnz}\cdots O_{Thz}$ and $C-H_{Bnz}\cdots Cl_{Dchlphy}$ hydrogen-bond energies are 134.3, 71.2 and 34.4 kJ mol^{-1}, respectively. Density functional theory (DFT) optimized structures at the B3LYP/6–311 G(d,p) level are compared with the experimentally determined molecular structure in the solid state. The HOMO–LUMO behaviour was elucidated to determine the energy gap. The two carbon atoms at the end of the nonyl chain are disordered in a 0.562 (4)/0.438 (4) ratio.

1. Chemical context

A number of sulfur- and nitrogen-containing heterocyclic compounds have been well studied. These molecules exhibit a wide range of biological applications, indicating that the 1,4-benzothiazine moiety is a potentially useful template in medicinal chemistry research with therapeutic applications in the antimicrobial (Armenise *et al.*, 2012, Sabatini *et al.*, 2008), anti-viral (Malagu *et al.*, 1998), anti-oxidant (Zia-ur-Rehman *et al.* 2009), anti-inflammatory (Trapani *et al.*, 1985; Gowda *et al.*, 2011) antipyretic (Warren *et al.*, 1987), and anti-cancer (Gupta *et al.*, 1991; Gupta *et al.*, 1985) areas as well as being precursors for the synthesis of new compounds (Sebbar *et al.*, 2015*a*; Vidal *et al.*, 2006) possessing anti-diabetic (Tawada *et al.*, 1990) and anti-corrosion activities (Ellouz *et al.*, 2016*a*,*b*; Sebbar *et al.*, 2016*a*) and biological properties (Hni *et al.*,

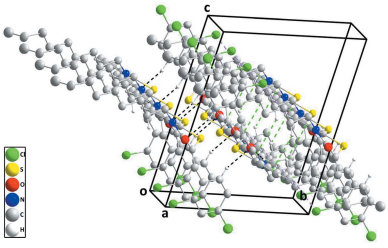

2019*a*; Ellouz *et al.*, 2017*a*,*b*, 2018; Sebbar *et al.*, 2019*a*,*b*). As a continuation of our research into the development of new 1,4-benzothiazine derivatives with potential pharmacological applications, we have studied the reaction of 1-bromononane with (*Z*)-2-(2,4-dichlorobenzylidene)-2*H*-1,4-benzothiazin-3(4*H*)-one under phase-transfer catalysis conditions using tetra-*n*-butylammonium bromide (TBAB) as catalyst and potassium carbonate as base (Hni *et al.*, 2019*b*; Sebbar *et al.*, 2019) to give the title compound, (I), in good yield. We report here its crystalline and molecular structures as well as the Hirshfeld surface analysis and the density functional theory (DFT) computational calculations.

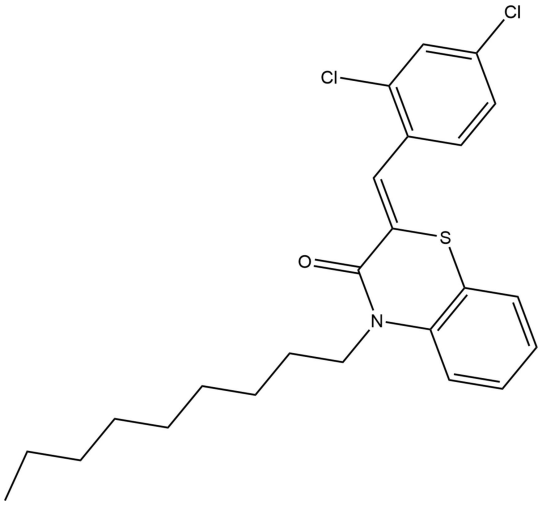

2. Structural commentary

The title compound contains 1,4-benzothiazine and 2,4-dichlorophenylmethylidene units (Fig. 1), in which the dihydrothiazine ring, *B* (S1/N1/C1/C6–C8), adopts a screw-boat conformation with puckering parameters Q_T = 0.5581 (16) Å, θ = 69.76 (18)° and φ = 334.3 (2)°. The planar rings, *A* (C1–C6) and *C* (C10–C15) are oriented at a dihedral angle of 88.45 (7)°.

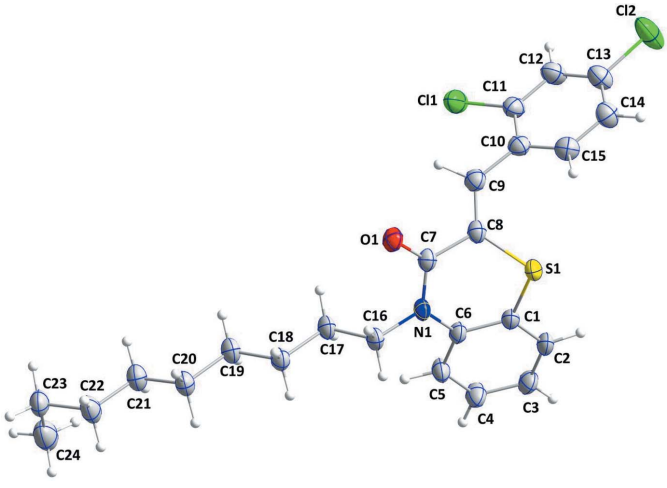

Figure 1
The molecular structure of the title compound with the atom-numbering scheme. Displacement ellipsoids are drawn at the 50% probability level.

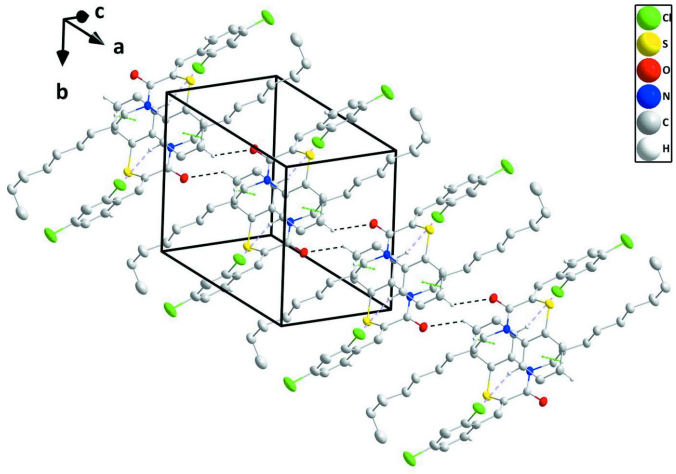

Figure 2
A perspective view of one double chain. The intermolecular C—$H_{Bnz}\cdots O_{Thz}$ and C—$H_{Bnz}\cdots Cl_{Dchlphy}$ (Bnz = benzene,Thz = thiazine and Dchlphy = 2,4-dichlorophenyl) hydrogen bonds are shown, respectively, as black and light purple dashed lines while the C—$H_{Dchlphy}\cdots\pi$ (ring) interactions are shown as green dashed lines.

Atoms Cl1, Cl2 and C9 are almost co-planar with ring *C* being displaced by 0.0247 (6), −0.0732 (9) and −0.0274 (2) Å, respectively.

3. Supramolecular features

In the crystal, C—$H_{Bnz}\cdots O_{Thz}$ (Bnz = benzene and Thz = thiazine) hydrogen bonds link the molecules, forming chains extending along the *a*-axis direction, which are connected to their inversion-related counterparts by C—$H_{Bnz}\cdots Cl_{Dchlphy}$ (Dchlphy = 2,4-dichlorophenyl) hydrogen bonds and C—$H_{Dchlphy}\cdots\pi$ (ring) interactions (Table 1 and Fig. 2). These double chains are further linked by C—$H_{Dchlphy}\cdots O_{Thz}$ hydrogen bonds to form stepped layers approximately parallel to (012) (Table 1 and Figs. 2 and 3).

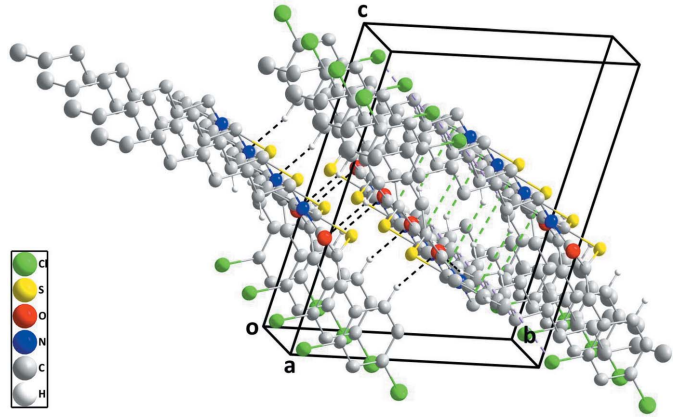

Figure 3
Perspective view of one double chain and half of a second showing the C—$H_{Dchlphy}\cdots O_{Thz}$ (Dchlphy = 2,4-dichlorophenyl and Thz = thiazine) hydrogen bond connecting them. Intermolecular interactions depicted as in Fig. 2.

Table 1
Hydrogen-bond geometry (Å, °).

*Cg*1 is the centroid of the ring *A* (C1–C6).

D—H···*A*	*D*—H	H···*A*	*D*···*A*	*D*—H···*A*
C3—H3···O1^{ix}	0.96 (3)	2.51 (3)	3.268 (2)	136 (2)
C5—H5···Cl1^{i}	0.96 (2)	2.86 (2)	3.634 (2)	138.8 (17)
C15—H15···O1^{vi}	0.96 (3)	2.36 (3)	3.270 (2)	159 (2)
C17—H17*A*···*Cg*1^{i}	0.98 (2)	2.90 (2)	3.619 (2)	131.2 (17)

Symmetry codes: (i) $-x+1, -y+1, -z+1$; (vi) $-x+1, -y, -z+1$; (ix) $x+1, y, z$.

4. Hirshfeld surface analysis

In order to visualize the intermolecular interactions in the crystal of the title compound, a Hirshfeld surface (HS) analysis (Hirshfeld, 1977; Spackman & Jayatilaka, 2009) was carried out by using *Crystal Explorer 17.5* (Turner *et al.*, 2017). In the HS plotted over d_{norm} (Fig. 4), the white surface indicates contacts with distances equal to the sum of van der Waals radii, and the red and blue colours indicate distances shorter (in close contact) or longer (distinct contact) than the van der Waals radii (Venkatesan *et al.*, 2016). The bright-red spots appearing near O1 and hydrogen atom H15 indicate their roles as the respective donors and/or acceptors; they also appear as blue and red regions corresponding to positive and negative potentials on the HS mapped over electrostatic potential (Spackman *et al.*, 2008; Jayatilaka *et al.*, 2005) as shown in Fig. 5. The blue regions indicate positive electrostatic potential (hydrogen-bond donors), while the red regions indicate negative electrostatic potential (hydrogen-bond acceptors). The shape-index of the HS is a tool to visualize π–π stacking by the presence of adjacent red and blue triangles; if there are no adjacent red and/or blue triangles, then there are no π–π interactions. Fig. 6 clearly suggests that there are no π–π interactions in (I). The overall two-dimensional fingerprint plot, Fig. 7*a*, and those delineated into H···H, C···H/H···C, Cl···H/H ··· Cl, O···H/H···O and S···H/H···S contacts (McKinnon *et al.*, 2007) are illustrated in Fig. 7*b*–*f*, respectively, together with their relative contributions to the Hirshfeld surface. The most important interaction is H···H (Table 2), contributing 44.7% to the overall crystal packing, which is reflected in Fig. 7*b* as widely scattered points of high density due to the large hydrogen content of the molecule with the tip at $d_e = d_i = 1.09$ Å. The presence of C—H···π interactions is indicated by the fringed pairs of characteristic wings in the fingerprint plot delineated into C···H/H···C contacts (Fig. 7*c*, 23.7% contribution to the HS). The two pairs of wings in the fingerprint plot delineated into

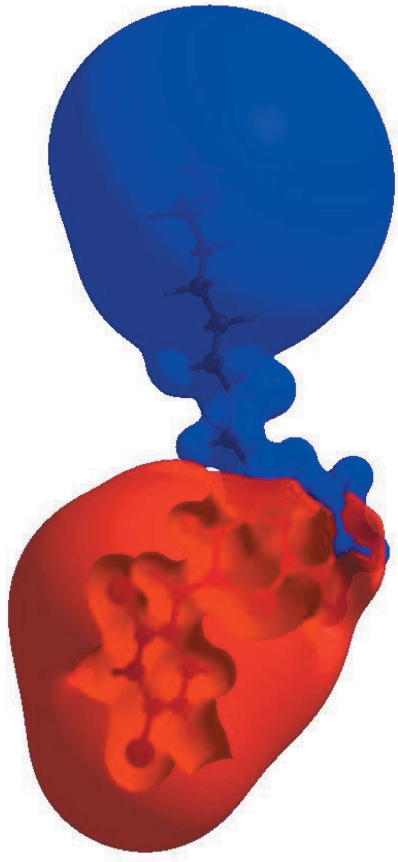

Figure 5
View of the three-dimensional Hirshfeld surface of the title compound plotted over electrostatic potential energy in the range −0.0500 to 0.0500 a.u. using the STO-3 G basis set at the Hartree–Fock level of theory. Hydrogen-bond donors and acceptors are shown as blue and red regions around the atoms corresponding to positive and negative potentials, respectively.

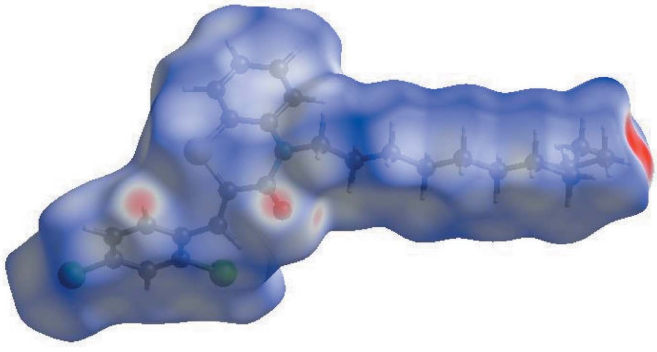

Figure 4
View of the three-dimensional Hirshfeld surface of the title compound plotted over d_{norm} in the range −0.6343 to 1.4076 a.u.

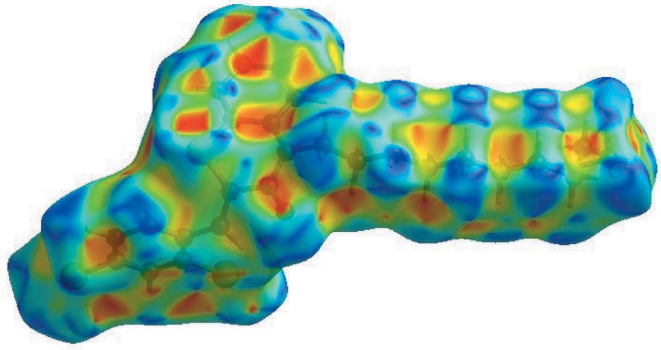

Figure 6
Hirshfeld surface of the title compound plotted over shape-index.

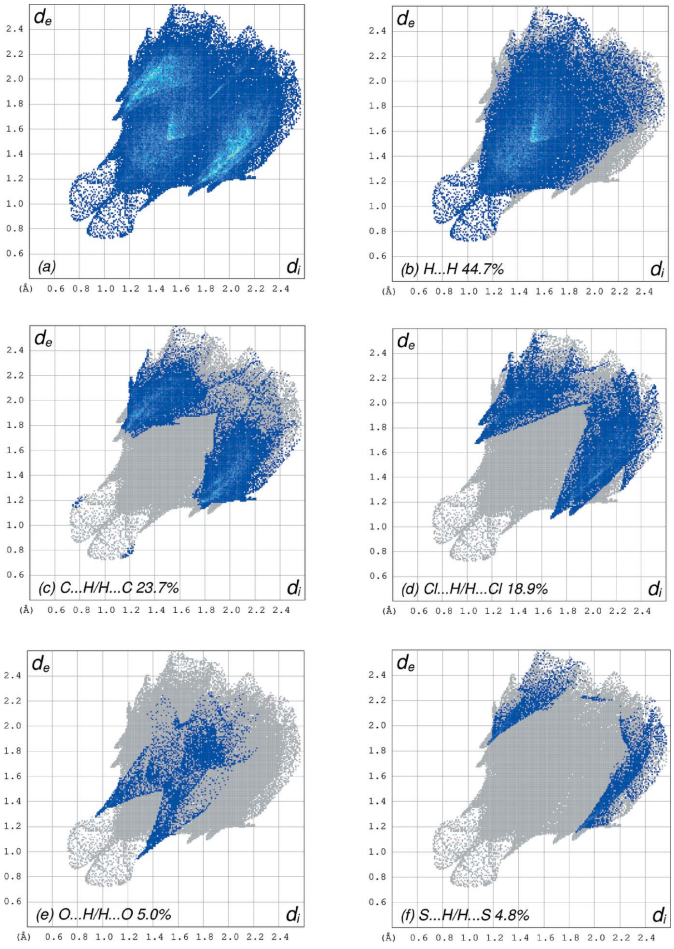

Figure 7
The full two-dimensional fingerprint plots for the title compound, showing (*a*) all interactions, and those delineated into (*b*) H···H, (*c*) C···H/H···C, (*d*) Cl···H/H···Cl, (*e*) O···H/H···O and (*f*) S···H/H···S contacts. The d_i and d_e values are the closest internal and external distances (in Å) from given points on the Hirshfeld surface contacts.

Cl···Hl/H···Cl contacts (Fig. 7*d*, 18.9% contribution) have an unsymmetrical distribution of points due to a third wing, with the edges at $d_e + d_i$ = 2.74 Å (for the long wing), $d_e + d_i$ = 2.92 Å (for the short wing) and $d_e + d_i$ = 3.53 Å (for the unsymmetrical third wing). The pair of wings in the fingerprint plot delineated into O···H/H···O contacts (Fig. 7*e*, 5.0% contribution) has a pair of spikes with the tips at $d_e + d_i$ = 2.22 Å. Finally, the wings in the fingerprint plot delineated into S···H/H···S contacts (Fig. 7*f*, 4.8% contribution) have the tips at $d_e + d_i$ = 2.99 Å.

The Hirshfeld surface representations with the function d_{norm} plotted onto the surface are shown for the H···H, C···H/H···C, Cl···H/H···Cl, O···H/H···O and S···H/H···S interactions in Fig. 8*a–e*, respectively.

The Hirshfeld surface analysis confirms the importance of H-atom contacts in establishing the packing. The large number of H···H, C···H/H···C, Cl···H/H···Cl and O···H/H···O interactions suggest that van der Waals interactions and hydrogen bonding play the major roles in the crystal packing (Hathwar *et al.*, 2015).

Table 2
Selected interatomic distances (Å).

Cl1···C5^{i}	3.634 (2)	C21···H24*B*	2.86
Cl1···C12^{ii}	3.548 (2)	C24···H21*B*	2.91
Cl1···H9	2.82 (3)	C24*A*···H24*E*^{viii}	2.44
Cl1···H5^{i}	2.86 (2)	C24*A*···H24*F*^{viii}	2.70
Cl1···H12^{ii}	2.92 (3)	C24*A*···H24*D*^{viii}	1.94
Cl2···H20*A*^{iii}	3.13 (2)	H3···H17*A*^{ix}	2.42 (4)
Cl2···H24*C*^{i}	3.01	H5···H17*B*	2.21 (4)
S1···N1	3.0439 (16)	H5···H16*B*	2.33 (3)
S1···C15	3.236 (2)	H12···H22*A*^{iii}	2.37
S1···H15	2.84 (3)	H16*A*···H18*A*	2.47 (3)
S1···H2^{iv}	3.15 (3)	H16*B*···H24*D*^{vii}	2.54
O1···C3^{v}	3.268 (2)	H16*B*···H18*B*	2.46 (3)
O1···C17	3.238 (2)	H16*B*···H24*A*^{vii}	2.49
O1···C15^{vi}	3.270 (2)	H17*A*···H19*A*	2.59 (3)
O1···H3^{v}	2.51 (3)	H17*B*···H19*B*	2.55 (4)
O1···H16*A*	2.43 (2)	H18*B*···H20*B*	2.55 (3)
O1···H17*A*	2.75 (2)	H19*A*···H21*A*	2.58 (4)
O1···H9	2.49 (3)	H19*B*···H21*B*	2.51 (4)
O1···H15^{vi}	2.36 (3)	H20*A*···H22*A*	2.49
C5···C17	3.430 (3)	H20*B*···H22*B*	2.54
C5···C24^{vii}	3.58	H21*A*···H23*B*	2.55
C6···C24^{vii}	3.58	H21*A*···H23*C*	2.60
C24*A*···C24*A*^{viii}	2.48	H21*B*···H24*B*	2.32
C2···H19*A*^{i}	2.98 (2)	H21*B*···H23*D*	2.34
C5···H24*A*^{vii}	2.99	H22*B*···H24*C*	2.27
C5···H16*B*	2.64 (2)	H22*B*···H24*E*	2.43
C5···H17*B*	2.93 (3)	H24*D*···C24*A*^{viii}	1.94
C7···H15^{vi}	2.95 (3)	H24*D*···H24*D*^{viii}	1.82
C7···H17*A*	2.99 (2)	H24*D*···H24*E*^{viii}	1.70
C16···H5	2.62 (3)	H24*D*···H24*F*^{viii}	2.07
C17···H3^{v}	2.98 (3)	H24*E*···H24*F*^{viii}	2.54
C17···H5	2.82 (3)		

Symmetry codes: (i) $-x+1, -y+1, -z+1$; (ii) $-x+1, -y, -z+2$; (iii) $x+1, y-1, z+1$; (iv) $-x+2, -y, -z+1$; (v) $x-1, y, z$; (vi) $-x+1, -y, -z+1$; (vii) $x+1, y-1, z$; (viii) $-x-1, -y+3, -z$; (ix) $x+1, y, z$.

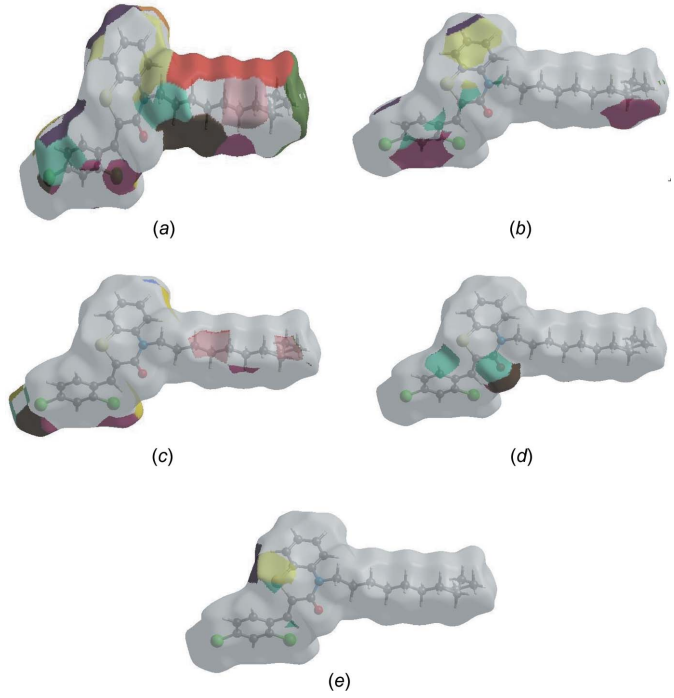

Figure 8
The Hirshfeld surface representations with the function d_{norm} plotted onto the surface for (*a*) H···H, (*b*) C···H/H···C, (*c*) Cl···H/H···Cl, (*d*) O···H/H···O and (*f*) S···H/H···S interactions.

Table 3
Comparison of the selected (X-ray and DFT) geometric data (Å, °).

Bonds/angles	X-ray	B3LYP/6–311G(d,p)
Cl1—C11	1.744 (2)	1.826
Cl2—C13	1.733 (2)	1.821
S1—C8	1.7578 (18)	1.831
S1—C1	1.7589 (18)	1.830
O1—C7	1.228 (2)	1.256
N1—C7	1.368 (2)	1.392
N1—C6	1.420 (2)	1.423
N1—C16	1.479 (2)	1.489
C8—S1—C1	97.27 (8)	99.15
C7—N1—C6	123.67 (14)	124.78
C7—N1—C16	117.19 (14)	114.70
C6—N1—C16	119.07 (15)	119.29
C2—C1—C6	120.22 (17)	121.21
C2—C1—S1	119.25 (13)	117.28
C6—C1—S1	120.52 (13)	121.48
C3—C2—S1	120.53 (17)	120.47

5. Interaction energy calculations

The intermolecular interaction energies were calculated using the CE–B3LYP/6–31G(d,p) energy model available in *Crystal Explorer 17.5* (Turner *et al.*, 2017), where a cluster of molecules is generated by applying crystallographic symmetry operations with respect to a selected central molecule within the default radius of 3.8 Å (Turner *et al.*, 2014). The total intermolecular energy (E_{tot}) is the sum of electrostatic (E_{ele}), polarization (E_{pol}), dispersion (E_{dis}) and exchange-repulsion (E_{rep}) energies (Turner *et al.*, 2015) with scale factors of 1.057, 0.740, 0.871 and 0.618, respectively (Mackenzie *et al.*, 2017). Hydrogen-bonding interaction energies (in kJ mol^{-1}) were calculated to be −53.7 (E_{ele}), −13.6 (E_{pol}), −161.9 (E_{dis}), 119.0 (E_{rep}) and −134.3 (E_{tot}) for C—$H_{Dchlphy}\cdots O_{Thz}$, 25.6 ($E_{ele}$), −5.7 ($E_{pol}$), −62.1 ($E_{dis}$), 23.1 ($E_{rep}$) and −71.2 ($E_{tot}$) [or C—$H_{Bnz}\cdots O_{Thz}$ and −16.0 (E_{ele}), −8.3 (E_{pol}), −43.0 (E_{dis}), 42.2 (E_{rep}) and −34.4 (E_{tot}) for C—$H_{Bnz}\cdots Cl_{Dchlphy}$ (Bnz = benzene, Thz = thiazine and Dchlphy = 2,4-dichlorophenyl).

6. DFT calculations

The optimized structure of the title compound, (I), in the gas phase was generated theoretically *via* density functional theory (DFT) using the standard B3LYP functional and 6–311G(d,p) basis-set calculations as implemented in *GAUSSIAN 09* (Frisch *et al.*, 2009). The theoretical and experimental results are in good agreement (Table 3). The highest-occupied molecular orbital (HOMO), acting as an electron donor, and the lowest-unoccupied molecular orbital (LUMO), acting as an electron acceptor, are very important parameters for quantum chemistry. When the energy gap is small, the molecule is highly polarizable and has high chemical reactivity. The DFT calculations provide some important information on the reactivity and site selectivity of the molecular framework. E_{HOMO} and E_{LUMO} clarify the inevitable charge-exchange collaboration inside the studied material, and together with the electronegativity (χ), hardness (η), potential (μ), electrophilicity (ω) and softness (σ) are recorded in Table 4. The

Table 4
Calculated energies.

Molecular Energy (a.u.) (eV)	Compound (I)
Total Energy, *TE* (eV)	−64734
E_{HOMO} (eV)	−6.9440
E_{LUMO} (eV)	−0.6941
Energy gap, ΔE (eV)	6.2499
Dipole moment, μ (Debye)	4.4939
Ionization potential, I (eV)	6.9440
Electron affinity, A	0.6941
Electro negativity, χ	3.8191
Hardness, η	3.1249
Electrophilicity index, ω	2.3337
Softness, σ	0.3200
Fraction of electron transferred, ΔN	0.5090

significance of η and σ is to evaluate both the reactivity and stability. The electron transition from the HOMO to the LUMO energy level is shown in Fig. 9. The HOMO and LUMO are localized in the plane extending from the whole (2*Z*)-2-[(2,4-dichlorophenyl)methylidene]-4-nonyl-3,4-dihydro-2*H*-1,4-benzothiazin-3-one ring.

7. Database survey

A search in the Cambridge Structural Database (Groom *et al.*, 2016; updated to October 2019), for compounds containing the fragment **II** gave 14 hits.

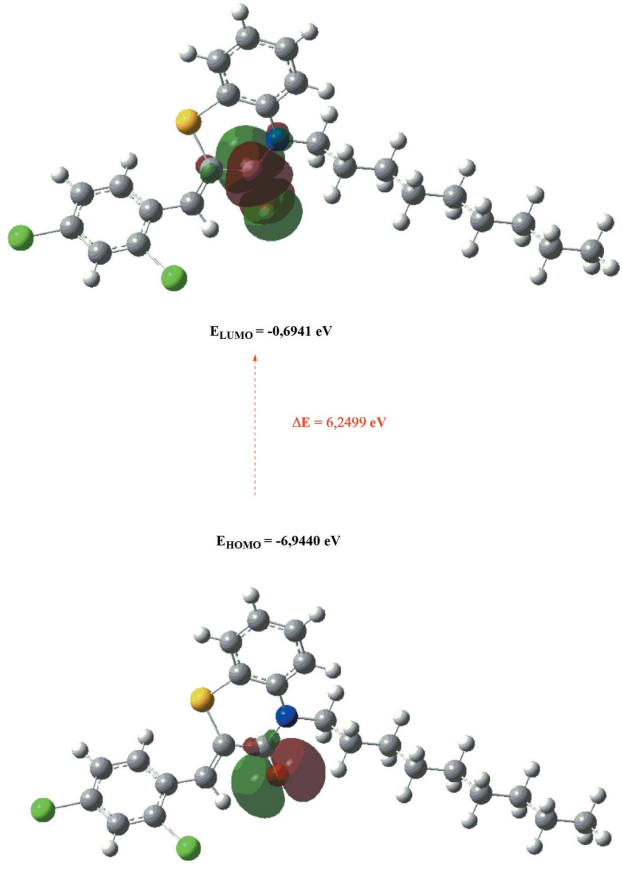

Figure 9
The energy band gap of the title compound.

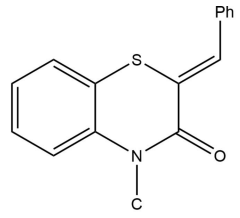

II

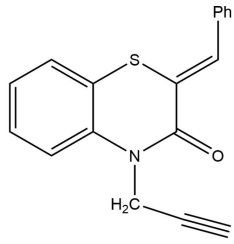

IIa

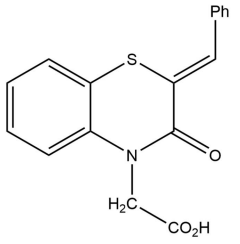

IIb

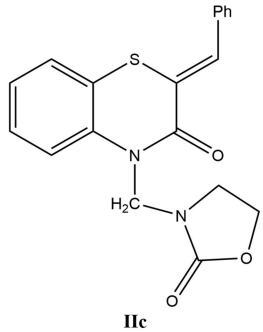

IIc

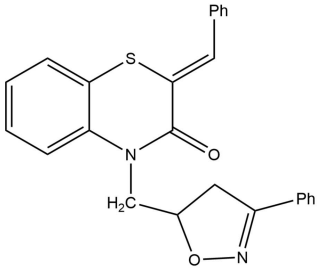

IId

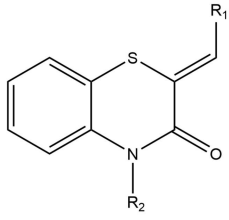

III

The largest set contains **IIa** (COGRUN; Sebbar *et al.*, 2014*a*), **IIb** (APAJUY; Sebbar *et al.*, 2016*c*), **IIc** (EVIYIT; Sebbar *et al.*, 2016*b*) and **IId** (WUFGIP; Sebbar *et al.*, 2015*b*). Additional examples are **III**: R_1 = 4-FC_6H_4 and R_2 = $CH_2C{\equiv}CH$ (WOCFUS; Hni *et al.*, 2019*a*), R_1 = 4-ClC_6H_4 and R_2 = CH_2Ph (OMEGEU; Ellouz *et al.*, 2016*c*) and R_1 = 2-ClC_6H_4, R_2 = $CH_2C{\equiv}CH$ (SAVTUH; Sebbar *et al.*, 2017). In all these compounds, the configuration about the benzylidene group: $C{=}CHC_6H_5$ bond is *Z*, and in the majority of these, the heterocyclic ring is quite non-planar with the dihedral angle between the plane defined by the benzene ring plus the nitrogen and sulfur atoms and that defined by nitrogen and sulfur and the other two carbon atoms separating them having approximate values of 36° (WUFGIP), 29° (APAJUY), 28° (SAVTUH), 26° (WOCFUS) and 25° (COGRUN). By contrast, in both EVIYIT and OMEGEU, the benzothiazine unit is nearly planar with the corresponding dihedral angle being about 4°.

8. Synthesis and crystallization

To a solution of (*Z*)-2-(2,4-dichlorobenzylidene)-2*H*-1,4-benzothiazin-3(4*H*)-one (1.5 mmol), potassium carbonate (2.7 mmol) and tetra-*n*-butyl ammonium bromide (0.14 mmol) in DMF (20 mL) was added 1-bromononane (2.6 mmol). Stirring was continued at room temperature for 24 h. The mixture was filtered and the solvent removed. The residue obtained was washed with water. The organic compound was chromatographed on a column of silica gel with ethyl acetate–hexane (9/1) as eluent. Colourless crystals were isolated when the solvent was allowed to evaporate (yield = 79%).

Table 5
Experimental details.

Crystal data	
Chemical formula	$C_{24}H_{27}Cl_2NOS$
M_r	448.42
Crystal system, space group	Triclinic, $P\overline{1}$
Temperature (K)	150
a, *b*, *c* (Å)	8.9961 (3), 10.3755 (3), 13.2565 (4)
α, β, γ (°)	73.857 (1), 88.119 (1), 74.182 (1)
V (Å^3)	1142.32 (6)
Z	2
Radiation type	Cu $K\alpha$
μ (mm^{-1})	3.52
Crystal size (mm)	0.20 × 0.14 × 0.08
Data collection	
Diffractometer	Bruker D8 VENTURE PHOTON 100 CMOS
Absorption correction	Multi-scan (*SADABS*; Krause *et al.*, 2015)
T_{min}, T_{max}	0.54, 0.76
No. of measured, independent and observed [$I > 2\sigma(I)$] reflections	8788, 4246, 3772
R_{int}	0.025
(sin $\theta/\lambda)_{max}$ (Å^{-1})	0.618
Refinement	
$R[F^2 > 2\sigma(F^2)]$, $wR(F^2)$, *S*	0.041, 0.107, 1.02
No. of reflections	4246
No. of parameters	349
No. of restraints	14
H-atom treatment	H atoms treated by a mixture of independent and constrained refinement
$\Delta\rho_{max}$, $\Delta\rho_{min}$ (e Å^{-3})	0.32, −0.50

Computer programs: *APEX3* and *SAINT* (Bruker, 2016), *SHELXT* (Sheldrick, 2015*a*), *SHELXL2018/1* (Sheldrick, 2015*b*), *DIAMOND* (Brandenburg & Putz, 2012) and *SHELXTL* (Sheldrick, 2008).

9. Refinement

Crystal data, data collection and structure refinement details are summarized in Table 5. The two carbon atoms at the end of the nonyl chain, C23 and C24, are disordered in a 0.562 (4)/0.438 (4) ratio. These were refined with restraints that the two components have comparable geometries. The H atoms on these carbons as well as those on C22 were included as riding contributions in idealized positions (C—H = 0.99 Å with U_{iso}(H) = 1.5U_{eq}(C).

Funding information

The support of NSF–MRI grant No. 1228232 for the purchase of the diffractometer and Tulane University for support of the Tulane Crystallography Laboratory are gratefully acknowledged. TH is grateful to Hacettepe University Scientific Research Project Unit (grant No. 013 D04 602 004).

References

Armenise, D., Muraglia, M., Florio, M. A., Laurentis, N. D., Rosato, A., Carrieri, A., Corbo, F. & Franchini, C. (2012). *Mol. Pharmacol. Mol. Pharmacol*, **50**, 1178–1188.

Brandenburg, K. & Putz, H. (2012). *DIAMOND*, Crystal Impact GbR, Bonn, Germany.

Bruker (2016). *APEX3*, *SAINT* and *SADABS*. Bruker AXS, Inc., Madison, Wisconsin, USA

Ellouz, M., Elmsellem, H., Sebbar, N. K., Steli, H., Al Mamari, K., Nadeem, A., Ouzidan, Y., Essassi, E. M., Abdel-Rahaman, I. & Hristov, P. (2016*b*). *J. Mater. Environ. Sci.* **7**, 2482–2497.

Ellouz, M., Sebbar, N. K., Boulhaoua, M., Essassi, E. M. & Mague, J. T. (2017*a*). *IUCr Data*, **2**, x170646.

Ellouz, M., Sebbar, N. K., Elmsellem, H., Steli, H., Fichtali, I., Mohamed, A. M. M., Mamari, K. A., Essassi, E. M. & Abdel-Rahaman, I. (2016*a*). *J. Mater. Environ. Sci.* **7**, 2806–2819.

Ellouz, M., Sebbar, N. K., Essassi, E. M., Ouzidan, Y., Mague, J. T. & Zouihri, H. (2016*c*). *IUCrData*, **1**, x160764.

Ellouz, M., Sebbar, N. K., Fichtali, I., Ouzidan, Y., Mennane, Z., Charof, R., Mague, J. T., Urrutigoïty, M. & Essassi, E. M. (2018). *Chem. Cent. J.* **12**, 123.

Ellouz, M., Sebbar, N. K., Ouzidan, Y., Essassi, E. M. & Mague, J. T. (2017*b*). *IUCr Data*, **2**, x170097.

Frisch, M. J., *et al.* (2009). *GAUSSIAN09*. Gaussian Inc., Wallingford, CT, USA.

Gowda, J., Khader, A. M. A., Kalluraya, B., Shree, P. & Shabaraya, A. R. (2011). *Eur. J. Med. Chem.* **46**, 4100.

Groom, C. R., Bruno, I. J., Lightfoot, M. P. & Ward, S. C. (2016). *Acta Cryst.* B**72**, 171–179.

Gupta, R. R., Kumar, R. & Gautam, R. K. (1985). *J. Fluor. Chem.* **28**, 381–385.

Gupta, V. & Gupta, R. R. (1991). *J. Prakt. Chem.* **333**, 153–156.

Hathwar, V. R., Sist, M., Jørgensen, M. R. V., Mamakhel, A. H., Wang, X., Hoffmann, C. M., Sugimoto, K., Overgaard, J. & Iversen, B. B. (2015). *IUCrJ*, **2**, 563–574.

Hirshfeld, H. L. (1977). *Theor. Chim. Acta*, **44**, 129–138.

Hni, B., Sebbar, N. K., Hökelek, T., El Ghayati, L., Bouzian, Y., Mague, J. T. & Essassi, E. M. (2019*b*). *Acta Cryst.* E**75**, 593–599.

Hni, B., Sebbar, N. K., Hökelek, T., Ouzidan, Y., Moussaif, A., Mague, J. T. & Essassi, E. M. (2019*a*). *Acta Cryst.* E**75**, 372–377.

Jayatilaka, D., Grimwood, D. J., Lee, A., Lemay, A., Russel, A. J., Taylor, C., Wolff, S. K., Cassam-Chenai, P. & Whitton, A. (2005). *TONTO - A System for Computational Chemistry. Available at: http://hirshfeldsurface.net/*

Krause, L., Herbst-Irmer, R., Sheldrick, G. M. & Stalke, D. (2015). *J. Appl. Cryst.* **48**, 3–10.

Mackenzie, C. F., Spackman, P. R., Jayatilaka, D. & Spackman, M. A. (2017). *IUCrJ*, **4**, 575–587.

Malagu, K., Boustie, J., David, M., Sauleau, J., Amoros, M., Girre, R. L. & Sauleau, A. (1998). *Pharm. Pharmacol. Commun.* **4**, 57–60.

McKinnon, J. J., Jayatilaka, D. & Spackman, M. A. (2007). *Chem. Commun.* pp. 3814–3816.

Sabatini, S., Kaatz, G. W., Rossolini, G. M., Brandini, D. & Fravolini, A. (2008). *J. Med. Chem.* **51**, 4321–4330.

Sebbar, N. K., Ellouz, M., Essassi, E. M., Ouzidan, Y. & Mague, J. T. (2015*a*). *Acta Cryst.* E**71**, o999.

Sebbar, N. K., Ellouz, M., Essassi, E. M., Saadi, M. & El Ammari, L. (2015*b*). *Acta Cryst.* E**71**, o423–o424.

Sebbar, N. K., Ellouz, M., Essassi, E. M., Saadi, M. & El Ammari, L. (2016*a*). *IUCr Data*.1, x161012.

Sebbar, N. K., Ellouz, M., Mague, J. T., Ouzidan, Y., Essassi, E. M. & Zouihri, H. (2016*c*). *IUCrData*, **1**, x160863.

Sebbar, N. K., Ellouz, M., Ouzidan, Y., Kaur, M., Essassi, E. M. & Jasinski, J. P. (2017). *IUCrData*, **2**, x170889.

Sebbar, N. K., Hni, B., Hökelek, T., Jaouhar, A., Labd Taha, M., Mague, J. T. & Essassi, E. M. (2019*a*). *Acta Cryst.* E**75**, 721–727.

Sebbar, N. K., Hni, B., Hökelek, T., Labd Taha, M., Mague, J. T., El Ghayati, L. & Essassi, E. M. (2019*b*). *Acta Cryst.* E**75**, 1650–1656.

Sebbar, N. K., Mekhzoum, M. E. M., Essassi, E. M., Zerzouf, A., Talbaoui, A., Bakri, Y., Saadi, M. & Ammari, L. E. (2016*b*). *Res. Chem. Intermed.* **42**, 6845–6862.

Sebbar, N. K., Zerzouf, A., Essassi, E. M., Saadi, M. & El Ammari, L. (2014*a*). *Acta Cryst.* E**70**, o614.

Sheldrick, G. M. (2008). *Acta Cryst.* A**64**, 112–122.

Sheldrick, G. M. (2015*a*). *Acta Cryst.* A**71**, 3–8.

Sheldrick, G. M. (2015*b*). *Acta Cryst.* C**71**, 3–8.

Spackman, M. A. & Jayatilaka, D. (2009). *CrystEngComm*, **11**, 19–32.

Spackman, M. A., McKinnon, J. J. & Jayatilaka, D. (2008). *Cryst. Eng. Comm*, **10**, 377–388.

Tawada, H., Sugiyama, Y., Ikeda, H., Yamamoto, Y. & Meguro, K. (1990). *Chem. Pharm. Bull.* **38**, 1238–1245.

Trapani, G., Reho, A., Morlacchi, F., Latrofa, A., Marchini, P., Venturi, F. & Cantalamessa, F. (1985). *Farm. Ed. Sci.* **40**, 369–376.

Turner, M. J., Grabowsky, S., Jayatilaka, D. & Spackman, M. A. (2014). *J. Phys. Chem. Lett.* **5**, 4249–4255.

Turner, M. J., McKinnon, J. J., Wolff, S. K., Grimwood, D. J., Spackman, P. R., Jayatilaka, D. & Spackman, M. A. (2017). *CrystalExplorer17*. The University of Western Australia.

Turner, M. J., Thomas, S. P., Shi, M. W., Jayatilaka, D. & Spackman, M. A. (2015). *Chem. Commun.* **51**, 3735–3738.

Venkatesan, P., Thamotharan, S., Ilangovan, A., Liang, H. & Sundius, T. (2016). *Spectrochim. Acta Part A*, **153**, 625–636.

Vidal, A., Madelmont, J. C. & Mounetou, E. A. (2006). *Synthesis*, pp. 591–593.

Warren, B. K. & Knaus, E. E. (1987). *Eur. J. Med. Chem.* **22**, 411–415.

Zia-ur-Rehman, M., Choudary, J. A., Elsegood, M. R. J., Siddiqui, H. L. & Khan, K. M. (2009). *Eur. J. Med. Chem.* **44**, 1311–1316.

supporting information

Acta Cryst. (2020). E**76**, 281-287 [https://doi.org/10.1107/S2056989020001036]

Crystal structure, Hirshfeld surface analysis, interaction energy and DFT studies of (2*Z*)-2-(2,4-dichlorobenzylidene)-4-nonyl-3,4-dihydro-2*H*-1,4-benzothiazin-3-one

Brahim Hni, Nada Kheira Sebbar, Tuncer Hökelek, Achour Redouane, Joel T. Mague, Noureddine Hamou Ahabchane and El Mokhtar Essassi

Computing details

Data collection: *APEX3* (Bruker, 2016); cell refinement: *SAINT* (Bruker, 2016); data reduction: *SAINT* (Bruker, 2016); program(s) used to solve structure: *SHELXT* (Sheldrick, 2015*a*); program(s) used to refine structure: *SHELXL2018/1* (Sheldrick, 2015*b*); molecular graphics: *DIAMOND* (Brandenburg & Putz, 2012); software used to prepare material for publication: *SHELXTL* (Sheldrick, 2008).

(2*Z*)-2-(2,4-Dichlorobenzylidene)-4-nonyl-3,4-dihydro-2*H*-1,4-benzothiazin-3-one

Crystal data

$C_{24}H_{27}Cl_2NOS$
M_r = 448.42
Triclinic, $P\overline{1}$
a = 8.9961 (3) Å
b = 10.3755 (3) Å
c = 13.2565 (4) Å
α = 73.857 (1)°
β = 88.119 (1)°
γ = 74.182 (1)°
V = 1142.32 (6) Å^3
Z = 2
$F(000)$ = 472
D_x = 1.304 Mg m^{-3}
Cu $K\alpha$ radiation, λ = 1.54178 Å
Cell parameters from 7317 reflections
θ = 3.5–72.4°
μ = 3.52 mm^{-1}
T = 150 K
Column, colourless
0.20 × 0.14 × 0.08 mm

Data collection

Bruker D8 VENTURE PHOTON 100 CMOS diffractometer
Radiation source: INCOATEC IμS micro-focus source
Mirror monochromator
Detector resolution: 10.4167 pixels mm^{-1}
ω scans
Absorption correction: multi-scan (*SADABS*; Krause *et al.*, 2015)
T_{min} = 0.54, T_{max} = 0.76
8788 measured reflections
4246 independent reflections
3772 reflections with $I > 2\sigma(I)$
R_{int} = 0.025
θ_{max} = 72.4°, θ_{min} = 3.5°
h = −10→11
k = −12→12
l = −13→15

Refinement

Refinement on F^2
Least-squares matrix: full
$R[F^2 > 2\sigma(F^2)]$ = 0.041
$wR(F^2)$ = 0.107
S = 1.01
4246 reflections
349 parameters
14 restraints

Primary atom site location: dual space
Secondary atom site location: difference Fourier map
Hydrogen site location: mixed
H atoms treated by a mixture of independent and constrained refinement

$w = 1/[\sigma^2(F_o^2) + (0.0512P)^2 + 0.6585P]$ where $P = (F_o^2 + 2F_c^2)/3$
$(\Delta/\sigma)_{max} < 0.001$
$\Delta\rho_{max} = 0.32$ e Å^{-3}
$\Delta\rho_{min} = -0.50$ e Å^{-3}

Special details

Geometry. All esds (except the esd in the dihedral angle between two l.s. planes) are estimated using the full covariance matrix. The cell esds are taken into account individually in the estimation of esds in distances, angles and torsion angles; correlations between esds in cell parameters are only used when they are defined by crystal symmetry. An approximate (isotropic) treatment of cell esds is used for estimating esds involving l.s. planes.

Refinement. Refinement of F^2 against ALL reflections. The weighted R-factor wR and goodness of fit S are based on F^2, conventional R-factors R are based on F, with F set to zero for negative F^2. The threshold expression of $F^2 > 2\text{sigma}(F^2)$ is used only for calculating R-factors(gt) etc. and is not relevant to the choice of reflections for refinement. R-factors based on F^2 are statistically about twice as large as those based on F, and R- factors based on ALL data will be even larger. The two carbons at the end of the nonyl chain, C23 and C24, are disordered in a 0.562 (4)/0.438 (4) ratio. These were refined with restraints that the two components have comparable geometries. The H-atoms on these carbons as well as those on C22 were included as riding contributions in idealized positions.

Fractional atomic coordinates and isotropic or equivalent isotropic displacement parameters (Å²)

	x	*y*	*z*	U_{iso}*/U_{eq}	Occ. (<1)
Cl1	0.49354 (7)	0.17182 (5)	0.85050 (4)	0.04871 (16)	
Cl2	0.90576 (10)	−0.32166 (6)	1.00981 (5)	0.0707 (2)	
S1	0.74621 (5)	0.09525 (4)	0.49738 (4)	0.03192 (13)	
O1	0.30841 (14)	0.26156 (14)	0.47052 (11)	0.0350 (3)	
N1	0.49478 (16)	0.35999 (15)	0.39383 (12)	0.0290 (3)	
C1	0.77339 (19)	0.26057 (18)	0.43712 (14)	0.0278 (4)	
C2	0.9224 (2)	0.2768 (2)	0.43323 (15)	0.0330 (4)	
H2	1.005 (3)	0.196 (3)	0.4656 (18)	0.042 (6)*	
C3	0.9469 (2)	0.4057 (2)	0.38810 (17)	0.0380 (4)	
H3	1.051 (3)	0.414 (3)	0.387 (2)	0.052 (7)*	
C4	0.8221 (2)	0.5199 (2)	0.34844 (18)	0.0410 (5)	
H4	0.837 (3)	0.613 (3)	0.316 (2)	0.056 (7)*	
C5	0.6730 (2)	0.5053 (2)	0.35211 (17)	0.0366 (4)	
H5	0.589 (3)	0.587 (2)	0.3270 (18)	0.039 (6)*	
C6	0.64689 (19)	0.37512 (19)	0.39486 (14)	0.0287 (4)	
C7	0.4449 (2)	0.26179 (18)	0.46805 (14)	0.0286 (4)	
C8	0.5633 (2)	0.15326 (18)	0.54591 (15)	0.0291 (4)	
C9	0.5205 (2)	0.1027 (2)	0.64295 (16)	0.0344 (4)	
H9	0.408 (3)	0.145 (3)	0.656 (2)	0.057 (7)*	
C10	0.6193 (2)	−0.0020 (2)	0.73085 (15)	0.0331 (4)	
C11	0.6141 (2)	0.0188 (2)	0.83067 (16)	0.0361 (4)	
C12	0.7034 (3)	−0.0761 (2)	0.91616 (17)	0.0418 (5)	
H12	0.700 (3)	−0.059 (3)	0.986 (2)	0.056 (7)*	
C13	0.8000 (3)	−0.1984 (2)	0.90162 (17)	0.0429 (5)	
C14	0.8106 (3)	−0.2233 (2)	0.80462 (17)	0.0407 (5)	
H14	0.880 (3)	−0.309 (3)	0.797 (2)	0.050 (7)*	
C15	0.7214 (2)	−0.1252 (2)	0.72000 (16)	0.0363 (4)	

H15	0.729 (3)	−0.149 (3)	0.655 (2)	0.046 (6)*	
C16	0.3799 (2)	0.4592 (2)	0.31152 (15)	0.0309 (4)	
H16A	0.315 (3)	0.405 (2)	0.2923 (17)	0.036 (6)*	
H16B	0.434 (2)	0.491 (2)	0.2491 (17)	0.028 (5)*	
C17	0.2769 (2)	0.5837 (2)	0.34303 (15)	0.0313 (4)	
H17A	0.225 (3)	0.548 (2)	0.4065 (18)	0.036 (6)*	
H17B	0.342 (3)	0.636 (2)	0.3630 (17)	0.032 (5)*	
C18	0.1618 (2)	0.6778 (2)	0.25291 (16)	0.0325 (4)	
H18A	0.104 (3)	0.623 (2)	0.2318 (17)	0.036 (6)*	
H18B	0.217 (3)	0.703 (2)	0.1916 (19)	0.040 (6)*	
C19	0.0581 (2)	0.8062 (2)	0.27852 (17)	0.0348 (4)	
H19A	0.004 (3)	0.776 (2)	0.3390 (18)	0.035 (6)*	
H19B	0.123 (3)	0.859 (3)	0.2959 (19)	0.045 (6)*	
C20	−0.0531 (2)	0.9040 (2)	0.18839 (17)	0.0372 (4)	
H20A	−0.125 (3)	0.853 (2)	0.1714 (18)	0.039 (6)*	
H20B	0.010 (3)	0.934 (2)	0.1228 (19)	0.043 (6)*	
C21	−0.1479 (2)	1.0373 (2)	0.21183 (18)	0.0383 (4)	
H21A	−0.205 (3)	1.011 (3)	0.274 (2)	0.059 (8)*	
H21B	−0.080 (3)	1.087 (2)	0.2266 (18)	0.042 (6)*	
C22	−0.2613 (3)	1.1333 (2)	0.12285 (19)	0.0493 (6)	
H22A	−0.325994	1.078902	0.104683	0.059*	
H22B	−0.201418	1.161858	0.060625	0.059*	
C23	−0.3697 (8)	1.2661 (4)	0.1422 (6)	0.0440 (18)	0.562 (4)
H23A	−0.458686	1.305117	0.090467	0.053*	0.562 (4)
H23B	−0.409306	1.245547	0.213838	0.053*	0.562 (4)
C24	−0.2717 (6)	1.3686 (5)	0.1297 (4)	0.0630 (10)	0.562 (4)
H24A	−0.335043	1.455992	0.141231	0.094*	0.562 (4)
H24B	−0.184022	1.328099	0.181244	0.094*	0.562 (4)
H24C	−0.233125	1.387336	0.058565	0.094*	0.562 (4)
C23A	−0.3282 (12)	1.2751 (6)	0.1453 (7)	0.0440 (18)	0.438 (4)
H23C	−0.388048	1.262316	0.209642	0.053*	0.438 (4)
H23D	−0.242430	1.312260	0.158121	0.053*	0.438 (4)
C24A	−0.4333 (8)	1.3801 (6)	0.0534 (5)	0.0630 (10)	0.438 (4)
H24D	−0.474134	1.469164	0.069938	0.094*	0.438 (4)
H24E	−0.373809	1.394060	−0.010101	0.094*	0.438 (4)
H24F	−0.519298	1.344161	0.041374	0.094*	0.438 (4)

Atomic displacement parameters (Å²)

	U^{11}	U^{22}	U^{33}	U^{12}	U^{13}	U^{23}
Cl1	0.0592 (3)	0.0364 (3)	0.0409 (3)	−0.0014 (2)	0.0109 (2)	−0.0080 (2)
Cl2	0.1011 (6)	0.0441 (3)	0.0459 (3)	0.0100 (3)	−0.0229 (3)	−0.0052 (2)
S1	0.0281 (2)	0.0251 (2)	0.0361 (3)	−0.00014 (16)	0.00197 (17)	−0.00517 (17)
O1	0.0233 (6)	0.0393 (7)	0.0427 (8)	−0.0097 (5)	−0.0023 (5)	−0.0104 (6)
N1	0.0200 (7)	0.0281 (7)	0.0351 (8)	−0.0032 (6)	−0.0043 (6)	−0.0054 (6)
C1	0.0231 (8)	0.0284 (8)	0.0289 (9)	−0.0028 (7)	0.0005 (6)	−0.0074 (7)
C2	0.0207 (8)	0.0363 (10)	0.0357 (10)	0.0002 (7)	−0.0005 (7)	−0.0076 (8)
C3	0.0217 (9)	0.0421 (11)	0.0473 (12)	−0.0077 (8)	0.0014 (8)	−0.0088 (9)

C4	0.0275 (9)	0.0339 (10)	0.0569 (13)	−0.0089 (8)	0.0019 (8)	−0.0049 (9)
C5	0.0244 (9)	0.0276 (9)	0.0502 (12)	−0.0032 (7)	−0.0027 (8)	−0.0020 (8)
C6	0.0198 (8)	0.0299 (9)	0.0338 (9)	−0.0038 (7)	−0.0009 (7)	−0.0076 (7)
C7	0.0248 (8)	0.0282 (8)	0.0336 (9)	−0.0058 (7)	−0.0016 (7)	−0.0111 (7)
C8	0.0248 (8)	0.0264 (8)	0.0359 (10)	−0.0063 (7)	−0.0018 (7)	−0.0087 (7)
C9	0.0295 (9)	0.0343 (10)	0.0384 (10)	−0.0093 (8)	0.0010 (8)	−0.0081 (8)
C10	0.0312 (9)	0.0335 (9)	0.0345 (10)	−0.0129 (8)	0.0021 (7)	−0.0055 (8)
C11	0.0403 (10)	0.0294 (9)	0.0358 (10)	−0.0091 (8)	0.0067 (8)	−0.0057 (8)
C12	0.0550 (13)	0.0372 (11)	0.0312 (11)	−0.0117 (9)	0.0019 (9)	−0.0077 (8)
C13	0.0527 (12)	0.0326 (10)	0.0382 (11)	−0.0078 (9)	−0.0058 (9)	−0.0045 (8)
C14	0.0463 (12)	0.0320 (10)	0.0434 (12)	−0.0083 (9)	−0.0026 (9)	−0.0117 (8)
C15	0.0402 (11)	0.0361 (10)	0.0361 (10)	−0.0141 (8)	0.0009 (8)	−0.0122 (8)
C16	0.0240 (8)	0.0312 (9)	0.0326 (10)	−0.0018 (7)	−0.0053 (7)	−0.0058 (7)
C17	0.0230 (8)	0.0306 (9)	0.0374 (10)	−0.0033 (7)	−0.0048 (7)	−0.0080 (8)
C18	0.0253 (9)	0.0322 (9)	0.0359 (10)	−0.0033 (7)	−0.0033 (8)	−0.0067 (8)
C19	0.0295 (9)	0.0320 (10)	0.0396 (11)	−0.0032 (8)	−0.0058 (8)	−0.0089 (8)
C20	0.0332 (10)	0.0318 (10)	0.0406 (11)	0.0006 (8)	−0.0052 (8)	−0.0088 (8)
C21	0.0350 (10)	0.0321 (10)	0.0440 (12)	−0.0017 (8)	−0.0041 (9)	−0.0113 (8)
C22	0.0505 (13)	0.0366 (11)	0.0476 (13)	0.0079 (10)	−0.0053 (10)	−0.0095 (9)
C23	0.033 (4)	0.0350 (13)	0.0547 (15)	0.0018 (17)	0.001 (2)	−0.0088 (11)
C24	0.064 (2)	0.0489 (19)	0.061 (2)	0.0064 (17)	−0.0022 (17)	−0.0126 (16)
C23A	0.033 (4)	0.0350 (13)	0.0547 (15)	0.0018 (17)	0.001 (2)	−0.0088 (11)
C24A	0.064 (2)	0.0489 (19)	0.061 (2)	0.0064 (17)	−0.0022 (17)	−0.0126 (16)

Geometric parameters (Å, º)

Cl1—C11	1.744 (2)	C16—H16B	0.97 (2)
Cl2—C13	1.733 (2)	C17—C18	1.528 (2)
S1—C8	1.7578 (18)	C17—H17A	0.98 (2)
S1—C1	1.7589 (18)	C17—H17B	0.98 (2)
O1—C7	1.228 (2)	C18—C19	1.521 (3)
N1—C7	1.368 (2)	C18—H18A	0.96 (2)
N1—C6	1.420 (2)	C18—H18B	0.95 (2)
N1—C16	1.479 (2)	C19—C20	1.519 (3)
C1—C2	1.393 (3)	C19—H19A	0.95 (2)
C1—C6	1.398 (2)	C19—H19B	0.97 (3)
C2—C3	1.379 (3)	C20—C21	1.522 (3)
C2—H2	0.96 (2)	C20—H20A	1.00 (2)
C3—C4	1.382 (3)	C20—H20B	1.04 (2)
C3—H3	0.96 (3)	C21—C22	1.515 (3)
C4—C5	1.388 (3)	C21—H21A	0.97 (3)
C4—H4	0.99 (3)	C21—H21B	0.96 (3)
C5—C6	1.392 (3)	C22—C23	1.537 (4)
C5—H5	0.96 (2)	C22—C23A	1.537 (4)
C7—C8	1.497 (2)	C22—H22A	0.9900
C8—C9	1.334 (3)	C22—H22B	0.9900
C9—C10	1.471 (3)	C23—C24	1.530 (7)
C9—H9	1.02 (3)	C23—H23A	0.9900

C10—C11	1.396 (3)	C23—H23B	0.9900
C10—C15	1.397 (3)	C24—H24A	0.9800
C11—C12	1.381 (3)	C24—H24B	0.9800
C12—C13	1.388 (3)	C24—H24C	0.9800
C12—H12	0.99 (3)	C23A—C24A	1.530 (8)
C13—C14	1.376 (3)	C23A—H23C	0.9900
C14—C15	1.385 (3)	C23A—H23D	0.9900
C14—H14	0.97 (3)	C24A—H24D	0.9800
C15—H15	0.96 (3)	C24A—H24E	0.9800
C16—C17	1.525 (3)	C24A—H24F	0.9800
C16—H16A	0.99 (2)		

Cl1···C5^{i}	3.634 (2)	C21···H24B	2.86
Cl1···C12^{ii}	3.548 (2)	C24···H21B	2.91
Cl1···H9	2.82 (3)	C24A···H24E^{viii}	2.44
Cl1···H5^{i}	2.86 (2)	C24A···H24F^{viii}	2.70
Cl1···H12^{ii}	2.92 (3)	C24A···H24D^{viii}	1.94
Cl2···H20A^{iii}	3.13 (2)	H3···H17A^{ix}	2.42 (4)
Cl2···H24C^{i}	3.01	H5···H17B	2.21 (4)
S1···N1	3.0439 (16)	H5···H16B	2.33 (3)
S1···C15	3.236 (2)	H12···H22A^{iii}	2.37
S1···H15	2.84 (3)	H16A···H18A	2.47 (3)
S1···H2^{iv}	3.15 (3)	H16B···H24D^{vii}	2.54
O1···C3^{v}	3.268 (2)	H16B···H18B	2.46 (3)
O1···C17	3.238 (2)	H16B···H24A^{vii}	2.49
O1···C15^{vi}	3.270 (2)	H17A···H19A	2.59 (3)
O1···H3^{v}	2.51 (3)	H17B···H19B	2.55 (4)
O1···H16A	2.43 (2)	H18B···H20B	2.55 (3)
O1···H17A	2.75 (2)	H19A···H21A	2.58 (4)
O1···H9	2.49 (3)	H19B···H21B	2.51 (4)
O1···H15^{vi}	2.36 (3)	H20A···H22A	2.49
C5···C17	3.430 (3)	H20B···H22B	2.54
C5···C24^{vii}	3.58	H21A···H23B	2.55
C6···C24^{vii}	3.58	H21A···H23C	2.60
C24A···C24A^{viii}	2.48	H21B···H24B	2.32
C2···H19A^{i}	2.98 (2)	H21B···H23D	2.34
C5···H24A^{vii}	2.99	H22B···H24C	2.27
C5···H16B	2.64 (2)	H22B···H24E	2.43
C5···H17B	2.93 (3)	H24D···C24A^{viii}	1.94
C7···H15^{vi}	2.95 (3)	H24D···H24D^{viii}	1.82
C7···H17A	2.99 (2)	H24D···H24E^{viii}	1.70
C16···H5	2.62 (3)	H24D···H24F^{viii}	2.07
C17···H3^{v}	2.98 (3)	H24E···H24F^{viii}	2.54
C17···H5	2.82 (3)		

C8—S1—C1	97.27 (8)	C16—C17—H17B	109.2 (13)
C7—N1—C6	123.67 (14)	C18—C17—H17B	110.8 (12)
C7—N1—C16	117.19 (14)	H17A—C17—H17B	106.0 (18)

C6—N1—C16	119.07 (15)	C19—C18—C17	113.07 (16)
C2—C1—C6	120.22 (17)	C19—C18—H18A	112.5 (13)
C2—C1—S1	119.25 (13)	C17—C18—H18A	109.3 (13)
C6—C1—S1	120.52 (13)	C19—C18—H18B	111.2 (14)
C3—C2—C1	120.53 (17)	C17—C18—H18B	108.8 (14)
C3—C2—H2	122.3 (14)	H18A—C18—H18B	101.4 (19)
C1—C2—H2	117.1 (14)	C20—C19—C18	113.91 (17)
C2—C3—C4	119.53 (18)	C20—C19—H19A	110.8 (14)
C2—C3—H3	118.7 (16)	C18—C19—H19A	108.3 (14)
C4—C3—H3	121.7 (16)	C20—C19—H19B	107.2 (14)
C3—C4—C5	120.51 (19)	C18—C19—H19B	108.7 (15)
C3—C4—H4	120.8 (16)	H19A—C19—H19B	107.7 (19)
C5—C4—H4	118.7 (16)	C19—C20—C21	113.55 (18)
C4—C5—C6	120.58 (17)	C19—C20—H20A	108.8 (13)
C4—C5—H5	118.4 (14)	C21—C20—H20A	109.2 (13)
C6—C5—H5	121.0 (14)	C19—C20—H20B	109.1 (13)
C5—C6—C1	118.59 (16)	C21—C20—H20B	107.1 (13)
C5—C6—N1	120.19 (15)	H20A—C20—H20B	109.1 (19)
C1—C6—N1	121.22 (16)	C22—C21—C20	113.53 (18)
O1—C7—N1	121.48 (16)	C22—C21—H21A	108.6 (17)
O1—C7—C8	121.01 (16)	C20—C21—H21A	107.9 (17)
N1—C7—C8	117.51 (15)	C22—C21—H21B	108.5 (14)
C9—C8—C7	118.51 (17)	C20—C21—H21B	109.6 (14)
C9—C8—S1	125.47 (14)	H21A—C21—H21B	109 (2)
C7—C8—S1	115.89 (13)	C21—C22—C23	117.2 (4)
C8—C9—C10	126.86 (18)	C21—C22—C23A	109.3 (4)
C8—C9—H9	114.5 (15)	C21—C22—H22A	108.0
C10—C9—H9	118.6 (15)	C23—C22—H22A	108.0
C11—C10—C15	116.75 (18)	C21—C22—H22B	108.0
C11—C10—C9	120.39 (18)	C23—C22—H22B	108.0
C15—C10—C9	122.85 (18)	H22A—C22—H22B	107.2
C12—C11—C10	122.93 (19)	C24—C23—C22	105.7 (4)
C12—C11—Cl1	117.26 (16)	C24—C23—H23A	110.6
C10—C11—Cl1	119.80 (15)	C22—C23—H23A	110.6
C11—C12—C13	117.9 (2)	C24—C23—H23B	110.6
C11—C12—H12	121.9 (16)	C22—C23—H23B	110.6
C13—C12—H12	120.1 (16)	H23A—C23—H23B	108.7
C14—C13—C12	121.42 (19)	C23—C24—H24A	109.5
C14—C13—Cl2	120.33 (17)	C23—C24—H24B	109.5
C12—C13—Cl2	118.25 (17)	H24A—C24—H24B	109.5
C13—C14—C15	119.3 (2)	C23—C24—H24C	109.5
C13—C14—H14	119.4 (15)	H24A—C24—H24C	109.5
C15—C14—H14	121.3 (15)	H24B—C24—H24C	109.5
C14—C15—C10	121.63 (19)	C24A—C23A—C22	111.3 (6)
C14—C15—H15	116.3 (15)	C24A—C23A—H23C	109.4
C10—C15—H15	121.9 (15)	C22—C23A—H23C	109.4
N1—C16—C17	115.05 (15)	C24A—C23A—H23D	109.4
N1—C16—H16A	106.7 (13)	C22—C23A—H23D	109.4

C17—C16—H16A	109.8 (13)	H23C—C23A—H23D	108.0
N1—C16—H16B	108.8 (12)	C23A—C24A—H24D	109.5
C17—C16—H16B	110.0 (12)	C23A—C24A—H24E	109.5
H16A—C16—H16B	106.0 (18)	H24D—C24A—H24E	109.5
C16—C17—C18	110.52 (16)	C23A—C24A—H24F	109.5
C16—C17—H17A	107.9 (13)	H24D—C24A—H24F	109.5
C18—C17—H17A	112.2 (13)	H24E—C24A—H24F	109.5

C8—S1—C1—C2	147.58 (16)	S1—C8—C9—C10	5.5 (3)
C8—S1—C1—C6	−31.51 (17)	C8—C9—C10—C11	133.9 (2)
C6—C1—C2—C3	0.2 (3)	C8—C9—C10—C15	−46.2 (3)
S1—C1—C2—C3	−178.87 (16)	C15—C10—C11—C12	−0.3 (3)
C1—C2—C3—C4	1.3 (3)	C9—C10—C11—C12	179.60 (19)
C2—C3—C4—C5	−1.1 (3)	C15—C10—C11—Cl1	178.39 (14)
C3—C4—C5—C6	−0.6 (4)	C9—C10—C11—Cl1	−1.7 (3)
C4—C5—C6—C1	2.1 (3)	C10—C11—C12—C13	−1.3 (3)
C4—C5—C6—N1	−177.04 (19)	Cl1—C11—C12—C13	179.99 (17)
C2—C1—C6—C5	−1.9 (3)	C11—C12—C13—C14	1.9 (3)
S1—C1—C6—C5	177.16 (15)	C11—C12—C13—Cl2	−177.07 (17)
C2—C1—C6—N1	177.25 (17)	C12—C13—C14—C15	−1.0 (3)
S1—C1—C6—N1	−3.7 (2)	Cl2—C13—C14—C15	178.02 (17)
C7—N1—C6—C5	−150.53 (19)	C13—C14—C15—C10	−0.7 (3)
C16—N1—C6—C5	26.4 (3)	C11—C10—C15—C14	1.3 (3)
C7—N1—C6—C1	30.3 (3)	C9—C10—C15—C14	−178.57 (19)
C16—N1—C6—C1	−152.76 (17)	C7—N1—C16—C17	82.7 (2)
C6—N1—C7—O1	172.26 (17)	C6—N1—C16—C17	−94.4 (2)
C16—N1—C7—O1	−4.7 (3)	N1—C16—C17—C18	−179.23 (15)
C6—N1—C7—C8	−8.3 (3)	C16—C17—C18—C19	−178.51 (17)
C16—N1—C7—C8	174.73 (16)	C17—C18—C19—C20	177.77 (17)
O1—C7—C8—C9	−32.8 (3)	C18—C19—C20—C21	−175.70 (18)
N1—C7—C8—C9	147.71 (18)	C19—C20—C21—C22	−178.7 (2)
O1—C7—C8—S1	143.15 (15)	C20—C21—C22—C23	176.0 (3)
N1—C7—C8—S1	−36.3 (2)	C20—C21—C22—C23A	−169.4 (5)
C1—S1—C8—C9	−133.86 (18)	C21—C22—C23—C24	78.1 (5)
C1—S1—C8—C7	50.47 (14)	C21—C22—C23A—C24A	175.2 (6)
C7—C8—C9—C10	−178.89 (17)		

Symmetry codes: (i) −*x*+1, −*y*+1, −*z*+1; (ii) −*x*+1, −*y*, −*z*+2; (iii) *x*+1, *y*−1, *z*+1; (iv) −*x*+2, −*y*, −*z*+1; (v) *x*−1, *y*, *z*; (vi) −*x*+1, −*y*, −*z*+1; (vii) *x*+1, *y*−1, *z*; (viii) −*x*−1, −*y*+3, −*z*; (ix) *x*+1, *y*, *z*.

Hydrogen-bond geometry (Å, º)

*Cg*1 is the centroid of the ring *A* (C1–C6).

D—H···*A*	*D*—H	H···*A*	*D*···*A*	*D*—H···*A*
C3—H3···O1^{ix}	0.96 (3)	2.51 (3)	3.268 (2)	136 (2)
C5—H5···Cl1^{i}	0.96 (2)	2.86 (2)	3.634 (2)	138.8 (17)

C15—H15···O1^{vi}	0.96 (3)	2.36 (3)	3.270 (2)	159 (2)
C17—H17*A*···*Cg*1^{i}	0.98 (2)	2.90 (2)	3.619 (2)	131.2 (17)

Symmetry codes: (i) −*x*+1, −*y*+1, −*z*+1; (vi) −*x*+1, −*y*, −*z*+1; (ix) *x*+1, *y*, *z*.